

UNIVERSITY OF HELSINKI

REPORT SERIES IN PHYSICS

HU-P-D101

**ELECTRONIC STRUCTURE OF MATTER
STUDIED BY COMPTON SCATTERING**

Simo Huotari

Division of X-ray Physics
Department of Physical Sciences
Faculty of Science
University of Helsinki
Helsinki, Finland

ACADEMIC DISSERTATION

*To be presented, with the permission of
the Faculty of Science of the University of Helsinki,
for public criticism in Auditorium E204 of
the Department of Physical Sciences (Physicum)
on 10th January 2003, at 12 o'clock.*

Helsinki 2002

ISBN 952-10-0565-3
ISSN 0356-0961
ISBN 952-10-0566-1 (pdf version)
<http://ethesis.helsinki.fi/>
Helsinki 2002
Yliopistopaino

Contents

1	Introduction	5
2	Compton scattering	7
2.1	Basics of non-resonant inelastic x-ray scattering	9
2.2	The impulse approximation	10
3	Description of the experiments	13
3.1	Beamline ID15B	13
3.2	Beamline ID16	15
3.3	The high-pressure cell	16
3.4	The gas cell	17
3.5	Data analysis	18
4	Electronic structure of matter	19
4.1	Atoms and molecules	20
4.2	Metals	24
5	Conclusions	29
6	Summary of the papers	30
	References	32

Preface

This thesis is based on research carried out at the Division of X-ray Physics of the Department of Physical Sciences at the University of Helsinki, and at the beamlines ID15B and ID16 of the European Synchrotron Radiation Facility (ESRF) in Grenoble, France.

I wish to thank Prof. Juhani Keinonen for providing me the opportunity to work at the Department of Physical Sciences. My special thanks belong to my supervisors Prof. Seppo Manninen and Prof. Keijo Hämäläinen for introducing me to the field of inelastic x-ray scattering and tutoring me throughout my studies. I wish also to express my gratitude to the personnel at the x-ray laboratory for creating both an encouraging and an inspiring working atmosphere. Especially I would like to thank Mr. Szabolcs Galambosi, Mr. Alekski Mattila, Dr. Jarkko Laukkanen, Dr. Alekski Soininen, and Dr. Sami Heinäsmäki for their important contribution in the research. I would also like to thank Dr. Christian Sternemann for invaluable discussions. The personnel of the European Synchrotron Radiation Facility has been of great help and support; especially without Dr. Thomas Buslaps the research could not have been feasible.

The work was funded by the National Graduate School of Materials Science, the Academy of Finland, the Finnish Academy of Science and Letters and the Foundation of Vilho, Yrjö and Kalle Väisälä.

S. Huotari: Electronic structure of matter studied by Compton scattering, University of Helsinki (2002), 39 pages + appendices. University of Helsinki, Report Series in Physics, HU-P-D101, ISSN 0356-0961, ISBN 952-10-0565-3, ISBN 952-10-0566-1 (pdf version).

Classification (INSPEC): A3220R, A3320R, A7125, A7110C

Keywords: electronic structure, inelastic x-ray scattering, Compton scattering, correlation

Abstract

Compton scattering is inelastic scattering of x rays from electrons. The information carried by the scattered photon is, within certain approximations, directly related to the velocity distribution of the scattering electron. Possible research topics include, for example, electron-electron correlation in all electron systems, as well as Fermi surfaces and electron-ion interaction in metals.

This work presents a systematic approach to study the electronic structure of matter utilizing high-resolution Compton scattering of synchrotron radiation. The main objective has been to gain an experimental measure of the strength of correlation effects in different electronic systems. For this purpose, Compton-scattering experiments were performed on various samples, starting from one of the simplest electronic systems, namely the helium atom, extending to the studies of the simple molecule N_2 and metallic systems sodium and beryllium. The experiments were carried out at the European Synchrotron Radiation Facility (ESRF) in Grenoble, France, utilizing two beamlines, namely ID16 for low-energy x rays (10 keV), and ID15B for high-energy x rays (30-60 keV). The results show deviations from calculations that have been generally regarded as highly accurate, especially in the case of inhomogeneous electron gas. This is a manifestation of the fact that correlation needs a more proper treatment in the calculations than is presently achievable.

List of publications

This thesis consists of an introductory part and the following scientific publications, which are referred to by Roman numerals **I** – **V** throughout the text.

I Simo Huotari, Keijo Hämäläinen, Seppo Manninen, Aretzki Issolah, and Massimiliano Marangolo: *Asymmetry of Compton profiles*, Journal of Physics and Chemistry of Solids **62**, 2205–2213 (2001)

II Simo Huotari, Keijo Hämäläinen, and Seppo Manninen: *Experimental determination of atomic wave functions: application on He*, submitted to Physical Review Letters

III Keijo Hämäläinen, Simo Huotari, Jarkko Laukkanen, Aleksi Soininen, Seppo Manninen, Chi-Chang Kao, Thomas Buslaps, and Mohammed Mezouar: *Free electron gas under high pressure*, Physical Review B **62**, R735–R738 (2000)

IV Simo Huotari, Keijo Hämäläinen, Seppo Manninen, Stanislaw Kaprzyk, Arun Bansil, Wolfgang Caliebe, Thomas Buslaps, Veijo Honkimäki, and Pekka Suortti: *Energy dependence of experimental Be Compton profiles*, Physical Review B **62**, 7956–7963 (2000)

V Simo Huotari, Keijo Hämäläinen, Seppo Manninen, Christian Sternemann, Axel Kaprolat, Winfried Schülke, and Thomas Buslaps: *High-momentum components and temperature dependence of the Compton profile of beryllium*, Physical Review B **66**, 085104-1–8 (2002)

1 Introduction

Compton scattering is a unique and a highly useful tool for electronic structure investigations. The mere discovery and correct interpretation [1] of Compton scattering represented a huge leap forward in our understanding of physics, because it was the Compton effect which proved that x rays can act not only as waves but also as particles, i.e. photons. For this experimental discovery Sir A. H. Compton was awarded the Nobel Prize in Physics in 1927. The triumph of the Compton effect continued when DuMond [2] used the Compton lineshape, i.e. the Compton profile, of beryllium to prove experimentally that electrons in a metal behave according to the newly-discovered Fermi-Dirac statistics, so belonging to the class of fermions. These studies were a significant part of the birth of quantum mechanics at the beginning of 20th century, and altered our view of the world irreversibly.

Unfortunately the experimental accuracy and feasibility of the experiments at that time were not very attractive to physicists, so the field of Compton scattering as a tool in electronic structure studies was practically forgotten for almost three decades. The revival of the Compton scattering technique took place in 1965 when Cooper *et al.* studied the Compton profile of Li metal using x-ray tubes and crystal analyzers [3]. Further development was provided by the introduction of solid-state detectors in the 1970's, making the experiments much easier to accomplish.

Other paths explored by inelastic x-ray scattering (IXS) studies were introduced by the discoveries of non-resonant Raman scattering [4] and resonant Raman scattering [5]. Hence Compton scattering became only one branch of IXS studies. Today IXS can be utilized in many different research areas [6], including the studies of phonons, plasmons, resonance phenomena, and valence-electron excitations. Furthermore, Compton scattering of elliptically-polarized photons (so-called magnetic Compton scattering) can be utilized as a very unique probe of the spin polarization of samples with magnetic properties [7–9].

The most recent advance in the field of Compton scattering studies has been due to the advent of high-brilliance synchrotron radiation sources, which allow feasible and accurate Compton-scattering experiments. The first pioneering studies were accomplished using solid-state detectors [10, 11], but soon also crystal spectrometers were introduced [12]. Novel experiments pushed the experimental resolution into a new level in the late 1990's, and the results were quite unexpectedly in large discrepancy with theoretical predictions [13]. This created a new level of activity in Compton scattering studies, which could be called the second Compton revival, and which this work is also a part of. Es-

pecially magnetic Compton scattering studies have been largely possible only due to the synchrotron radiation sources, which are able to provide highly intense elliptically polarized radiation. The development has culminated in the high-resolution spectrometers currently installed at beamlines around the world. Today, Compton scattering experiments are quite well presented in the field of condensed-matter physics [14–44].

The birth of synchrotron radiation sources has been a success story of its own [45]. Synchrotron radiation was first considered a nuisance in particle accelerators, because it diminished the energy of the charged particles in the accelerator rings. However, it was soon realized that the bending magnets of the synchrotrons could be used as a source of high-intensity radiation in the x-ray range, and x-ray physicists could use the particle accelerators as parasites. These sources are now known as first-generation synchrotron radiation sources. Later on, synchrotrons purely dedicated for producing radiation were built constituting the second generation of synchrotron radiation sources. So-called insertion devices, i.e. wigglers and undulators, were installed into the straight sections of the second-generation storage rings, providing much brighter radiation than the old bending magnets. This led to the birth of the third-generation synchrotron radiation sources, like the European Synchrotron Radiation Facility (ESRF), where this work was accomplished at. These synchrotrons were optimized primarily for the insertion devices. The scientific community is currently working on the fourth generation of synchrotron radiation sources, for which a strong candidate is the free-electron laser, proposed to reach photon energies of ~ 10 keV [46].

As is the case generally in science, theoretical and experimental studies have had a very intensive dialog in the history of IXS. Sometimes experimentalists have discovered new phenomena with no obvious theoretical explanation and this has led theoretical studies forward. On the other hand, theoretical predictions have been made that have demanded a completely new level of accuracy from the experiments. This work is a part of the systematic experimental and theoretical studies of (i) electronic structure of matter in its various forms and (ii) the Compton-scattering process as an interaction of x rays and electrons. These studies have brought information not only on electrons and electromagnetic radiation but also, indirectly, on ions in matter as well.

One of the most important problems in solid-state physics and also a main topic in this thesis is electron-electron correlation. The simplest approximation in an electron system taking into account the Pauli exclusion principle between fermions is the Hartree-Fock approximation. However, the Coulombic repulsion between electrons is only taken into account in this approximation statically, i.e. when calculating the behavior of an electron in a system with N electrons, the states of the other $N - 1$ electrons are assumed not

to change due to the electron under study. The dynamic response of the other electrons, neglected in the Hartree-Fock approximation, is called correlation. Since the electron density in a solid-state system is $\sim 10^{23}/\text{cm}^3$, the effects of correlation are quite difficult to calculate exactly. Moreover, correlation effects can be difficult to separate from such factors as the electron-ion interaction, finite-temperature effects and final-state effects in the scattering process. This work is a contribution to the research of these effects in electron systems.

This thesis is divided into five parts. The present section constitutes of a brief review on the history and literature of Compton scattering. In the Section 2 a brief introduction to the theoretical background of the scattering process is given. The Section 3 describes the relevant experimental details of the beamline constructions, sample environments and data analysis procedures. The background for understanding the electronic structure of the investigated samples as well as the main results are given in the Section 4. Finally, the Sections 5 and 6 give a short summary of the main results of the present work.

The unit system adopted in this thesis is the atomic unit (a.u.) system, where $\hbar = m = e = 1$. The atomic unit for length is the Bohr radius a_0 (0.529 Å) and for momentum $1/a_0$ ($1.993 \cdot 10^{-24}$ kgm/s). Photon energies are represented in electron volts (eV).

2 Compton scattering

Most of the experimental tools utilized in solid-state physics are based on scattering or absorption of photons, electrons, positrons, neutrons or other particles. The interaction between the probe and the system under study gives information on the properties of the system, provided that the theory of the interaction itself is known well enough. A particle impinging on a system creates an excitation and finally leaves the system with its momentum, and sometimes also its energy and the polarization state changed. If the energy of the probe changes, the scattering process is inelastic. In this case also the final state of the system is different from its initial state, the energy difference between the states being equal to the energy change of the probing particle. Relevant excitations and energy ranges that can be probed with the inelastic scattering techniques are numerous, and consist of phonons (~ 1 meV), plasmons (~ 10 eV), core-electron excitations (~ 100 eV– 10 keV) and Compton scattering of high-energy x rays (~ 10 keV), just to mention a few examples.

The amount of momentum transferred to the system determines the type of excitation in question. In the low-momentum transfer regime the excitations are mainly of a many-particle (collective) kind. These can be, for example, phonons, plasmons, magnons, etc.

In the high-momentum transfer region, the probe sees the particle as independent and thus single-particle modes can be excited.

This thesis reports studies of the scattering of x rays from electrons when the energy and momentum transfers are large compared to characteristic energies and momenta of the scattering electrons, and when the incident-photon energy is far from resonances of the electron system (absorption edges, etc). This branch of inelastic x-ray scattering is called *Compton scattering*, and the following analysis will be confined to this specific regime. For a review of other types of inelastic x-ray scattering, the reader is referred to Ref. [47].

Compton scattering can be used to the investigations of the momentum density of the electrons [48, 49]. Perhaps a somewhat more widely used concept is the charge density $\rho(\mathbf{r})$, measured as the absolute square of the electron wave function in position space, $\psi(\mathbf{r})$. The momentum density $N(\mathbf{p})$ is correspondingly the square of the electron wave function $\chi(\mathbf{p})$ in Fourier, or momentum, space:

$$\rho(\mathbf{r}) = |\psi(\mathbf{r})|^2 \quad (1)$$

$$N(\mathbf{p}) = |\chi(\mathbf{p})|^2, \quad (2)$$

where the wave functions are coupled through the Fourier transform,

$$\chi(\mathbf{p}) = (2\pi)^{-3/2} \int d\mathbf{r} \psi(\mathbf{r}) e^{i\mathbf{p}\cdot\mathbf{r}} \quad (3)$$

$$\psi(\mathbf{r}) = (2\pi)^{-3/2} \int d\mathbf{p} \chi(\mathbf{p}) e^{-i\mathbf{p}\cdot\mathbf{r}} \quad (4)$$

Momentum densities of electron systems can also be measured using the positron-annihilation [50], $(\gamma, e\gamma)$ [51], and $(e, 2e)$ [52] spectroscopic methods. These competing techniques have their own advantages and disadvantages over Compton spectroscopy. The positron-annihilation method requires perfect single crystals, and especially clean surfaces. The $(e, 2e)$ and $(\gamma, e\gamma)$ methods are limited to gases or very thin foils due to a high probability of multiple scattering of the electrons. All these methods are surface sensitive, whereas Compton scattering probes the bulk material and does not require perfectly clean surfaces or thin samples. Thus the Compton scattering method can be applied to all electronic systems, whether they are in a gaseous, liquid, or solid form. However, Compton scattering can only provide a one-dimensional projection of the momentum density, whereas the competing methods can be applied to measure two-dimensional projections. The three-dimensional momentum density can be reconstructed by measuring several directional Compton profiles of single-crystalline samples and applying reconstruction methods based on e.g. Fourier analysis [44, 53].

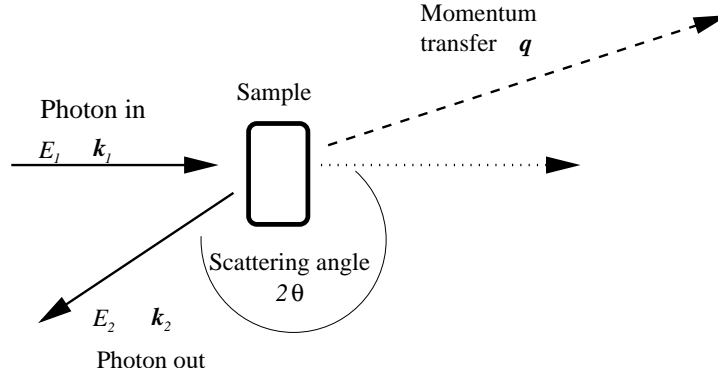


Figure 1: Representation of the scattering process.

2.1 Basics of non-resonant inelastic x-ray scattering

In a photon-electron scattering process a photon with an incident energy E_1 , a wave vector \mathbf{k}_1 and a polarization state $\hat{\mathbf{e}}_1$ collides with an electron possessing a momentum \mathbf{p} and an energy ϵ_i . The final state has an electron with a momentum $\mathbf{p} + \mathbf{q}$ and an energy ϵ_f , and a photon with an energy E_2 , a wave vector \mathbf{k}_2 and a polarization state $\hat{\mathbf{e}}_2$. The energy transferred by the photon to the electron is denoted by $E = E_1 - E_2$ and the momentum transfer by $\mathbf{q} = \mathbf{k}_1 - \mathbf{k}_2$.

The probability for a scattering event is proportional to the double-differential cross section, which, when far from all resonances of the system, can be written non-relativistically as [54]

$$\frac{d^2\sigma}{d\Omega dE_2} = r_e^2 \frac{E_2}{E_1} (\hat{\mathbf{e}}_1 \cdot \hat{\mathbf{e}}_2)^2 \sum_{i,f} \left| \langle f | \sum_{\alpha} e^{i\mathbf{q}\cdot\mathbf{r}_{\alpha}} | i \rangle \right|^2 \delta(E + \epsilon_i - \epsilon_f), \quad (5)$$

where r_e is the classical electron radius. The summations are taken over all electrons in the system, located at \mathbf{r}_{α} , and over all initial and final states $|i\rangle$ and $|f\rangle$. The first part of the cross section is the Thomson cross section,

$$\left(\frac{d\sigma}{d\Omega} \right)_{\text{Th}} = r_e^2 \frac{E_2}{E_1} (\hat{\mathbf{e}}_1 \cdot \hat{\mathbf{e}}_2)^2. \quad (6)$$

The second part of the cross section is called the dynamic structure factor,

$$S(\mathbf{q}, E) = \sum_{i,f} \left| \langle f | \sum_{\alpha} e^{i\mathbf{q}\cdot\mathbf{r}_{\alpha}} | i \rangle \right|^2 \delta(E + \epsilon_i - \epsilon_f). \quad (7)$$

Using these conventions, the double-differential scattering cross section can be written as

$$\frac{d^2\sigma}{d\Omega dE_2} = \left(\frac{d\sigma}{d\Omega} \right)_{\text{Th}} S(\mathbf{q}, E). \quad (8)$$

2.2 The impulse approximation

The dynamic structure factor is related to the electron-density fluctuations in the sample. The physical meaning is best shown by the representation of van Hove [55],

$$S(\mathbf{q}, E) = \frac{N}{2\pi} \int_{-\infty}^{\infty} dt \int d\mathbf{r} e^{i(\mathbf{q}\cdot\mathbf{r}-Et)} G(\mathbf{r}, t), \quad (9)$$

where $G(\mathbf{r}, t)$ is the pair distribution function of the electrons, and N is the number of particles in the system. From this formulation it can be seen that the physical meaning of the dynamic structure factor is to be the Fourier transform of the pair distribution function over space and time. Relevant limits to $S(\mathbf{q}, E)$ are (a being the length scale of the system, e.g. the average distance between neighboring atoms)

- $q \approx 1/a$: The dynamic structure factor does not change appreciably within different positions in space, and thus collective excitations are observed.
- $q \gg 1/a$: Different particles scatter independently, and one-electron excitations can be observed.

When the momentum and energy transfers are large, the dynamic structure factor can be approximated further to reach a very important result [56]. Expressing the delta function in (7) in its Fourier integral representation, the dynamic structure factor can be rewritten as

$$S(\mathbf{q}, E) = \frac{1}{2\pi} \int_{-\infty}^{\infty} dt e^{iEt} \sum_{i,f} \langle i | e^{iHt} \sum_{\alpha} e^{-i\mathbf{q}\cdot\mathbf{r}_{\alpha}} e^{-iHt} | f \rangle \langle f | \sum_{\alpha} e^{i\mathbf{q}\cdot\mathbf{r}_{\alpha}} | i \rangle. \quad (10)$$

Now we can make the approximation (H_0 being the Hamiltonian for a free electron and V the potential due to the nucleus),

$$e^{i(H_0+V)t} = e^{iH_0t} e^{iVt} e^{-[H_0,V]t^2/2} \dots \approx e^{iH_0t} e^{iVt}. \quad (11)$$

The last form is valid if the time scale of the scattering process is very short with respect to the relaxation times of the system, so that the scattering happens very fast, or the energy transfer is large. Assuming that the final states form a complete set, the dynamic structure factor can be written as

$$S(\mathbf{q}, E) \approx \frac{1}{2\pi} \sum_i \int_{-\infty}^{\infty} dt e^{iEt} \sum_{\alpha} \langle i | e^{iH_0t} e^{-i\mathbf{q}\cdot\mathbf{r}_{\alpha}} e^{-iH_0t} e^{i\mathbf{q}\cdot\mathbf{r}_{\alpha}} | i \rangle. \quad (12)$$

The potential V has disappeared from the expression above. This does not mean that it is approximated to zero, but rather that it cancels out between the initial and final

states. Another way of looking at this is that if the scattering process is very fast, the electron has no time to react before the photon is already scattered away. Hence, the scattered photon can carry no information about the final state of the electron. This approximation is called the impulse approximation (IA) and it is essential to the analysis of Compton-scattered photons. From the last expression we can approximate further [56],

$$S(\mathbf{q}, E) \approx \sum_{\alpha} \int d\mathbf{p}_{\alpha} |\chi(\mathbf{p}_{\alpha})|^2 \delta(E - \mathbf{q} \cdot \mathbf{p}_{\alpha} - \frac{1}{2}q^2). \quad (13)$$

From this, the momentum density of the electron $N(\mathbf{p}_{\alpha}) = |\chi(\mathbf{p}_{\alpha})|^2$ can be recognized. By choosing the z -axis of the momentum \mathbf{p}_{α} to be along the vector \mathbf{q} , the integral is easily computed due to the delta function. We will drop the summation and the index α for clarity, and assume that $N(\mathbf{p})$ is the sum of the momentum densities of all electrons:

$$S(\mathbf{q}, E) \approx \frac{1}{q} \int_{-\infty}^{\infty} \int_{-\infty}^{\infty} dp_x dp_y N(\mathbf{p}) = \frac{1}{q} J(p_z), \quad (14)$$

where we have defined the Compton profile

$$J(p_z) = \int_{-\infty}^{\infty} \int_{-\infty}^{\infty} dp_x dp_y N(\mathbf{p}). \quad (15)$$

The correspondence of the scattered photon energy and p_z can be calculated from relativistic kinematics and is [57]

$$p_z = \frac{q}{2} - (E_1 - E_2) \sqrt{\frac{1}{4} + \frac{c^4}{2E_1 E_2 (1 - \cos \phi)}}. \quad (16)$$

An example of a Compton profile is presented in Figure 2, which shows the experimental and theoretical Compton profiles of Be. The contributions of the 1s and 2s electrons are shown separately. Since the scattering process is incoherent, electrons give additive contributions to the scattering cross section and thus the Compton profile is the sum of the profiles of the individual occupied orbitals.

The usual argument to justify the validity of the IA is that for the scattering process to be fast, the energy transferred to the system should be large compared to the binding energy of the electrons [56]. The highest energy transfer utilized in this work was 10 keV (corresponding the backscattering geometry for an incident photon energy of 56 keV), and even with these energies the Compton profile of the 1s electrons of Be (binding energy 111 eV) exhibits an notable asymmetry due to the failure of the IA.

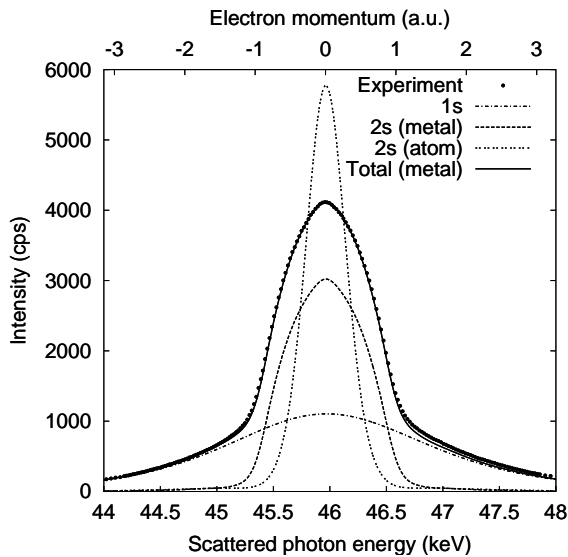


Figure 2: Example of how the energy spectrum of the scattered photons is transformed to the Compton profile in the momentum scale. The sample was a Be single crystal with the scattering vector along the $[100]$ reciprocal lattice vector. The dashed and dashed-dotted lines correspond to theoretical results by Bansil *et al.* [58–60] for metallic Be. The dotted line is the free-atom $2s$ profile [61] as an example of how sensitive the $2s$ profile is to the chemical environment. The incident energy is 56 keV, scattering angle 173° and the mean energy transfer 10 keV. The slight asymmetry in the experimental profile is due to the failure of the impulse approximation for the $1s$ electrons, and the excess of electrons above -1 and 1 a.u. is possibly due to electron-electron correlation effects.

There have been several studies to calculate and measure the effect of this phenomenon on Compton profiles [62–68]. As a result, it is generally agreed that the failure of the IA causes the Compton profiles to become asymmetric, but on quantitative level the agreement of experimental and theoretical results is not yet satisfactory. On the experimental side, asymmetry can also be caused by incorrect data analysis, background, multiple scattering, misalignment of the experimental apparatus, etc. Especially the separation of the asymmetry due to the failure of the IA and the asymmetry caused by multiple scattering can be difficult.

The failure of the IA can be divided into two categories, the valence electron and the core electron parts (**paper I**). It was found out that the valence electron Compton profile can exhibit asymmetry and smearing of the Fermi surface signatures if the energy transfer is of the order of 500 eV (the mean energy transfer in backscattering geometry for $E_1 \approx 10$ keV). The valence electron part had no asymmetry when the provided energy transfer was 3 keV or more. It can thus be concluded that for the IA to be valid for the valence electrons in metals, the minimum energy-transfer value lies between these two limits. This is rather surprising, since the binding energy of these electrons is only a few electron volts. This fact is crucial, because it is often the valence electrons that the solid-state physicist is interested in, and these results suggest that it may not be possible to arbitrarily enhance the accuracy of the experiment if the transferred energy is below the 3 keV limit, due to the failure of the underlying approximations. Recently this effect

was also observed by Sternemann *et al.* in lithium [69], and the effect has been lately studied also theoretically [69–72].

The Be 1s (core electron) Compton profile was found to exhibit asymmetry due to the failure of the IA even with the highest energy-transfer value reached, i.e. 10 keV, as can be seen from Figure 2. Fortunately, the core electron contribution does not contain sharp structures, and while the core electrons are rather uninteresting from the point of view of solid-state physics, their contribution can be quite easily subtracted from the signal even when the IA is not valid. For this purpose, the asymmetric core-electron Compton profile needs to be found, either accurately by calculation or empirically from experiment. A rather good theoretical treatment to account for the failures of IA is the quasi-self-consistent-field (QSCF) method by Issolah *et al.* [62, 63]. The results of this method and another one, a simple analytical expression for the first order correction to the Compton profiles [64], were compared to the experimental asymmetries in the **paper I**. It was discovered that the QSCF produced a reasonable, but by no means perfect, agreement with the experimental results. This suggests that a more sophisticated method is needed to account for the failure of the IA.

3 Description of the experiments

The experimental work for this thesis was done at the European Synchrotron Radiation Facility (ESRF) beamlines ID15B and ID16. The beamline ID15B [73, 74] is capable of producing monochromatic high-energy radiation (29–90 keV) with a flux of about 10^{12} monochromatic photons/s at the sample, while ID16 is built to produce lower-energy photons (\sim 7–25 keV) with a roughly similar intensity. Both beamlines are designed for inelastic x-ray scattering studies, but differ from each other in several ways. Besides ID16 being optimized for lower energy photons than ID15B and having a different kind of insertion device, it differs from ID15B by the possibility to change the energy of incident photons continuously.

3.1 Beamline ID15B

The radiation source at ID15B was a seven-period asymmetric permanent-magnet wiggler, which has a critical energy of 44.1 keV. The radiation was monochromatized by bent focusing Si monochromators with a demagnification ratio of 5:1. At present, the beamline has three separate monochromators installed, which can be operated one at a time. Thus the beamline is able to provide photons with energies of 29 keV, 56 keV and 90 keV. In this

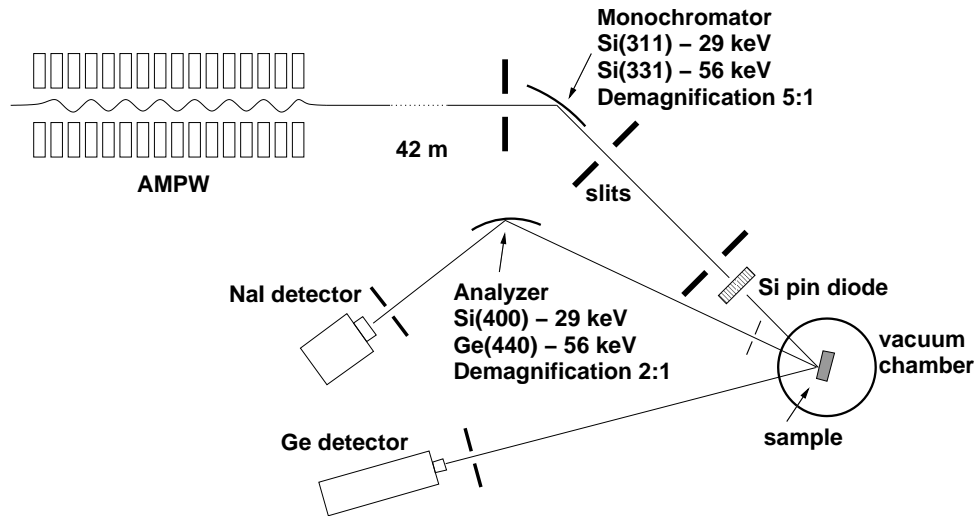


Figure 3: Layout of the experimental station ID15B.

work, energies of 29 keV and 56 keV were used. The monochromators were Si(111) and Si(311), respectively. The monochromators also acted as horizontally focusing elements. The beam was cut with heavy-metal slits into a vertical line up to 5.0 mm high and 0.3 mm wide, the width essentially determining the resolution of the instrument due to the angle-dispersive nature of the crystal spectrometer. A Si PIN diode was installed before the sample to monitor the incident-photon flux and operated in the photovoltaic (current) mode.

The spectra of the scattered x rays were recorded using a scanning crystal spectrometer, except in the case of the high-pressure studies, where the spectra were recorded using a Ge solid-state detector due to a low counting rate. The Ge detector has a poorer energy resolution but is more efficient in terms of intensity than the spectrometer. Whenever the spectra were recorded using the scanning crystal spectrometer, the Ge detector was used together with the Si PIN diode to monitor the intensity of the incident photon beam by recording the integrated intensity of photons scattered from the sample. As a monitor it has the advantage that it is possible to separate the signal from the nominal Si(111) reflection at $E_1 = 29$ keV from the signal due to the third harmonic, i.e. the Si(333) reflection having the energy of 87 keV. With the Si PIN diode operating in the photovoltaic mode it was not possible to separate photons with different energies. This is crucial since the intensity ratio of the Si(333) reflection to the Si(111) reflection was not constant but changed with the heatload of the monochromator, and hence as a function of time. With the Si(311) reflection ($E_1 = 56$ keV) the third harmonic did not have a significant role, since the intensity of the 180 keV radiation coming from the wiggler source was minimal, especially after the monochromator since the reflecting power of the monochromator is

very small for these high-order reflections. The drawback of the solid-state detector is that it is limited by statistical accuracy and it has a smaller dynamic range than the current-mode Si PIN diode.

The spectrometer operated in Rowland geometry and was based on cylindrically bent Si(400) and Ge(440) crystals, for incident photon energies of 29 and 56 keV, respectively. The crystals were asymmetrically cut to obtain a demagnification ratio of 2:1. The intensity of the reflected radiation was recorded with a NaI scintillation detector. The spectrometer was controlled with the computer program `spec` [75]. The scattering angle for the spectrometer was 173° and for the Ge detector 160° .

The factor that dominated the instrumental resolution function in the experiments utilizing the scanning crystal spectrometer was the illuminated effective sample size. In the experiments where Be single crystals were used as samples, the resolution function in momentum space had a full-width-at-half-maximum (FWHM) of 0.08 a.u. for $E_1 = 29$ keV and 0.16 a.u. for $E_1 = 56$ keV. The resolution in the case of gaseous samples was lower since the illuminated sample volume was not that well confined. By utilizing the focusing properties of the spectrometer and narrow slitting, a resolution function with a FWHM of 0.3 a.u. was achieved. In the high-pressure studies, where a solid-state Ge detector was used, the momentum resolution was dominated by the energy resolution of the detector. The resolution function for this experiment had a FWHM of approximately 0.6 a.u. in momentum space.

3.2 Beamline ID16

The beamline ID16 is designed for high-resolution studies of electronic excitations and phonons. It is used primarily for low energy-transfer studies (from 1 meV to a few eV), and the possibility to scan the large energy range needed in Compton spectrometry (in this case, ~ 1 keV) posed a challenge of its own. The radiation source at ID16 consisted of two consecutive undulators, and the radiation was monochromatized using two Si(111) crystals. The double-crystal monochromator made it possible to change the incident-photon energy continuously without the beam moving significantly. The undulators and the monochromator were operated synchronously with the `spec` [75] computer program. The utilized incident-photon energy E_1 was tuned between 9.9 and 10.9 keV. At this beamline the so-called inverse geometry was utilized, i.e. the scattered photon energy was kept fixed and the incident-photon energy was scanned through the energy region of interest. The spectrometer operated at a nearly backscattering geometry (Bragg angle 86°) with a Si(555) analyzer crystal. A vacuum chamber was installed in the beam path to minimize air absorption.

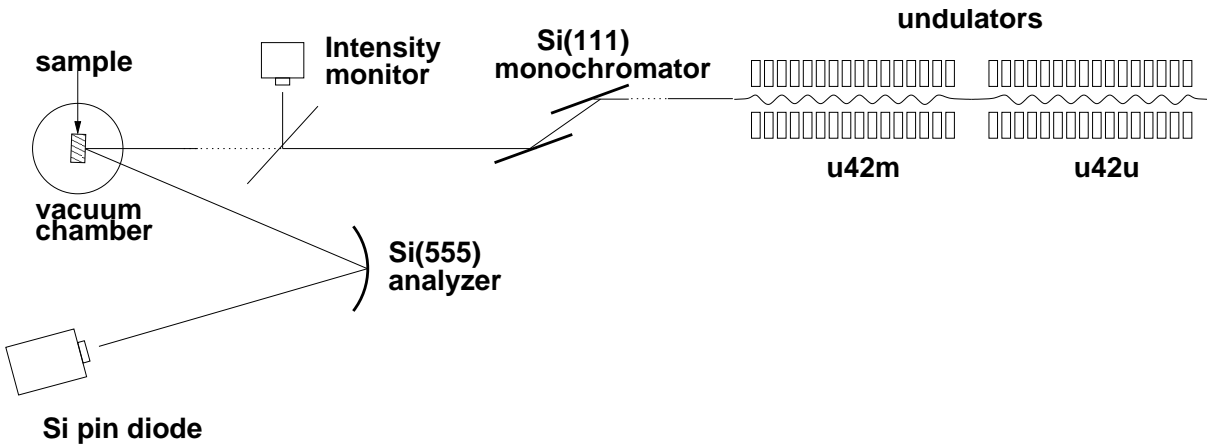


Figure 4: Layout of the experimental station ID16.

It is possible to measure the intensity of scattered radiation with a fixed monochromatic energy as a function of the incident-photon energy, because in non-resonant x-ray scattering the incident-photon energy can be chosen somewhat arbitrarily. This is not the case for example in resonant scattering experiments, where the physics of the scattering process change appreciably over even a small energy range. The advantage of this method, compared to the scanning crystal spectrometer, is that the spectrometer becomes easier to operate since it does not require movement and there is no need to correct for the analyzer crystal and detector efficiencies with different photon energies. However, monitoring the incident-beam intensity becomes now an energy-dependent problem. Widely used ionization chambers would be quite easy to operate and the efficiency as a function of incident-photon energy could be calculated quite accurately, but at ID16 their usability is rather limited. This is due to the fact that the photon flux is so high and the beam so well focused that the response of the ion chamber is no longer linear, and is very sensitive to fluctuations in the beam shape and size. In this experiment the incident-beam intensity was monitored by using a thin Kapton foil installed in the beam path, and a PIN diode recording the number of photons scattered by the foil.

The resolution of the instrument at ID16 was mainly determined by the solid angle seen by the analyzer crystal, i.e. the uncertainty of the scattering angle. In momentum space the resolution function had a FWHM of 0.02 a.u.

3.3 The high-pressure cell

The **paper III** describes an experiment to measure the density dependence of the electronic properties of free electron gas. In practice this was done by applying a high pressure

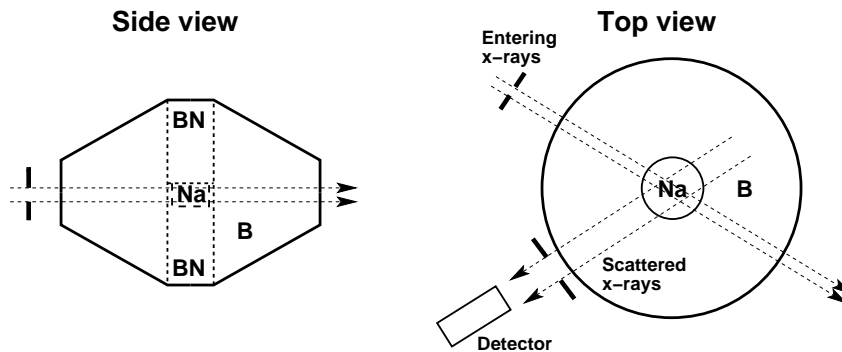


Figure 5: Schematic presentation of the LVC sample gasket for studying materials under high pressure.

to a Na sample and then measuring its Compton profile with $E_1 = 56$ keV at ID15B. The pressure was applied by using a mechanical Paris-Edinburgh large-volume cell (LVC) press [76, 77]. The highest pressure used was 4.2 GPa. The sample was enclosed within a gasket made out of boron epoxy, which is a hard material but quite opaque for high-energy x rays. The sample is stored inside the boron gasket and enclosed within a boron nitride capsule. Boron nitride, in turn, is a soft material which ensures that the pressure within the sample is uniform. The sample gasket is presented in Figure 5.

While the pressures attainable with the large-volume cell press are of the order of a few GPa's, much higher pressures (up to 300 GPa) have been reached by using diamond anvil cells [78, 79]. An attempt to accomplish the high-pressure experiment with a diamond anvil cell was also made. Besides offering higher pressures, it is a small, hand-held device and thus would be also more practical in experiments than the large volume cell. However, the sample volume in the diamond anvil cell was too small compared to the incident beam size and the focusing power of the spectrometer, resulting in ~ 60 % of the measured signal to originate from the diamond anvils. Vertical focusing and an optimization of the focusing properties of the spectrometer would probably make further experiments with the diamond anvil cells feasible. A new construction of moissanite (hexagonal silicon carbide) anvil cell was recently reported to allow sample sizes of three orders of magnitude larger than in diamond anvil cells [80]. The achieved pressure was 50 GPa, so this new cell could be the next step toward more accurate Compton scattering experiments under high pressure.

3.4 The gas cell

The gaseous systems He and N₂ were studied at ID15B utilizing a gas cell, which is schematically presented in Figure 6. The utilized incident photon energy was $E_1 =$

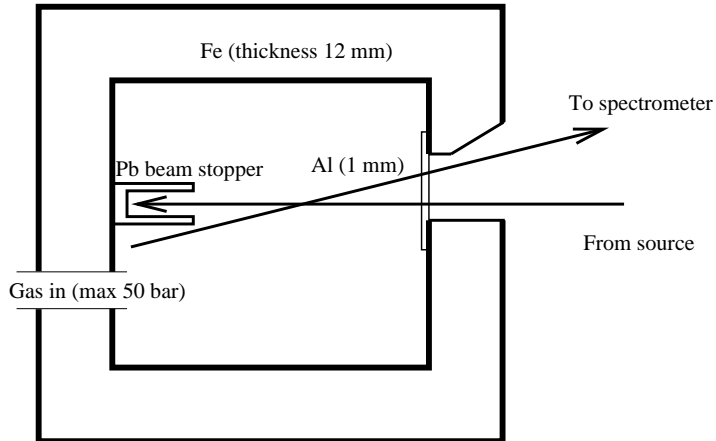


Figure 6: Overview of the gas cell in which the gaseous materials were studied.

56 keV. The gas cell was originally used by Paakkari *et al.* [81], and slightly modified for our studies. The utilized gas pressure was 50 bar and its purpose was to increase the count rate. This pressure does not affect the electronic properties of the atoms or molecules under study. The cell was made of stainless steel and the entrance/exit window was covered with a 1-mm thick Al plate. A Pb beam stopper was installed to minimize multiple scattering events, which could take place from the walls of the gas cell.

3.5 Data analysis

Numerous issues have to be taken into account before the data recorded by the detector can be analyzed as a Compton profile. The most important ones are the conversion of the cross-section (as a function of scattered photon energy) to the Compton profile (as a function of p_z), background subtraction, and corrections for the detector and the analyzer crystal efficiency, absorption in the sample and air, dead time effects, and multiple scattering.

The Compton profile was calculated from the measured cross section using the relativistic formulation of Holm [57]. The efficiencies of the analyzer crystals were taken into account by calculating the reflectivity curves using a lamellar model [82]. The background was measured whenever possible (e.g. empty gas cell) or was approximated as linear.

One crucial factor in the data analysis is the intensity normalization. Although the ESRF is a very reliable photon source, the intensity of incident photons still changes appreciably during the course of the experiment and has to be monitored. Unfortunately this is not always such a simple task. The monitoring elements can be affected by higher-order harmonic reflections from the monochromators, beam movement, dead time, etc. This poses a problem especially because the heatload of the optical elements of the

beamlines changes with time, combined to the fact that the detectors may suffer from a dead time effect (the dynamic range of the detector being too small). In all experiments, the spectra were measured several times and they were ensured to be identical after normalization and dead-time corrections, within the statistical accuracy.

4 Electronic structure of matter

This thesis comprises of a systematic comparison of experimental and theoretical Compton profiles of electronic systems with a varying level of complicity. For this purpose, a series of Compton-scattering experiments was accomplished with samples ranging from the simplest possible system that can be feasibly measured, namely the He atom, up to a much more complicated system, namely the inhomogeneous electron gas of Be. Systems with much higher level of complicity, for example high- T_C superconductors, can also be studied by the Compton scattering method [28,39] but they are out of the scope of this thesis.

When discussing the electronic structure of matter, a distinction to the so-called core and valence electrons is usually made. In solid-state physics the electrons of interest are usually the valence electrons, since they carry the information necessary to understand most transport phenomena and e.g. optical properties of the system. On the other hand, the core electrons can in some cases be used as an indirect probe, for example in the studies of defects in semiconductors [83]. In solid-state systems also the tightly bound core electrons are affected by the crystal potential, and their wave functions are modified from the free-atom wave functions, mainly due to the fact that they have to be orthogonal to the valence-electron wave functions. Thus truly atomic systems can only be studied in their non-solid (preferably gaseous) state.

The Compton profile of helium was measured as described in the **paper II**, and the studies were later extended to the N_2 molecule [84]. Both systems were studied in the gaseous state. A more complicated system, the free-electron gas, was studied in the **paper III**, which describes a Compton-scattering study on Na in high pressure. The valence electrons of Na serve as a free electron gas to a good approximation, so in this study the interaction between the valence electrons and the ions can be neglected. To study this interaction, a two-fold study of the valence electron structure of beryllium metal was performed, as described in the **papers IV** and **V**.

One of the main topics of this thesis is electron-electron correlation. i.e. all interactions that are not accounted for in the Hartree-Fock approximation. Correlation and its effect on electron systems are among the most important problems in many-body

physics [85,86]. An exact calculation of correlation effects in solids is quite difficult and approximations are evidently necessary. Also electron-ion interaction, i.e. band structure, can have effects on the electronic states that are similar to the effects of correlation, so these effects can be difficult to separate from each other. On the other hand, the helium atom constitutes only a three-particle problem and can thus be modeled quite accurately. We would thus expect a quite good agreement between experimental and theoretical Compton profiles of He, and more discrepancies when we reach inhomogeneous electron gas, like the valence electrons of metallic Be.

4.1 Atoms and molecules

The many-particle wave function is in the Hartree-Fock approximation a Slater determinant [87,88] (for simplicity, the following analysis will be confined to closed-shell systems):

$$\Psi(\mathbf{r}_1, \mathbf{r}_2, \dots, \mathbf{r}_{2N}, \mathbf{s}_1, \mathbf{s}_2, \dots, \mathbf{s}_{2N}) =$$

$$\begin{vmatrix} \psi_1(\mathbf{r}_1)\alpha(\mathbf{s}_1) & \psi_1(\mathbf{r}_1)\beta(\mathbf{s}_1) & \psi_2(\mathbf{r}_1)\alpha(\mathbf{s}_1) & \dots & \psi_{2N}(\mathbf{r}_1)\alpha(\mathbf{s}_1) \\ \psi_1(\mathbf{r}_2)\alpha(\mathbf{s}_2) & \psi_1(\mathbf{r}_2)\beta(\mathbf{s}_2) & \psi_2(\mathbf{r}_2)\alpha(\mathbf{s}_2) & \dots & \psi_{2N}(\mathbf{r}_2)\alpha(\mathbf{s}_2) \\ \vdots & \vdots & \vdots & \ddots & \vdots \\ \psi_1(\mathbf{r}_{2N})\alpha(\mathbf{s}_{2N}) & \psi_1(\mathbf{r}_{2N})\beta(\mathbf{s}_{2N}) & \psi_2(\mathbf{r}_{2N})\alpha(\mathbf{s}_{2N}) & \dots & \psi_{2N}(\mathbf{r}_{2N})\beta(\mathbf{s}_{2N}) \end{vmatrix}$$

where the spatial parts of the individual orbitals are denoted as $\psi_i(\mathbf{r}_j)$ and the spin parts as $\alpha(\mathbf{s}_j)$ and $\beta(\mathbf{s}_j)$. The spin parts of the orbitals are complete and orthogonal with respect to integration in the spin space, i.e. the summation over possible spin values,

$$\sum_{\mathbf{s}} \alpha(\mathbf{s})\beta^\dagger(\mathbf{s}) = 0 \quad (17)$$

$$\sum_{\mathbf{s}} \alpha(\mathbf{s})\alpha^\dagger(\mathbf{s}) = \sum_{\mathbf{s}} \beta(\mathbf{s})\beta^\dagger(\mathbf{s}) = 1. \quad (18)$$

As the orbitals $\psi_i(\mathbf{r})$ are orthogonal as well (being solutions to the same Schrödinger equation), the charge density is

$$\rho(\mathbf{r}) = \sum_i \rho_i(\mathbf{r}) = 2 \sum_i |\psi_i(\mathbf{r})|^2. \quad (19)$$

An often used method to calculate the wave functions of atomic and molecular systems is the linear combination of atomic orbitals (LCAO) method, which assumes that the orbitals $\psi_i(\mathbf{r}_j)$ can be taken to be linear combinations of primitive orbitals,

$$\psi_i(\mathbf{r}_j) = \sum_{\mu} c_{i\mu} \phi_{\mu}(\mathbf{r}_j). \quad (20)$$

The primitive orbitals are sometimes chosen to be Slater functions,

$$\phi_{nlm}(\mathbf{r}_j) = R_{nl}(r)Y_{lm}(\theta, \varphi) \quad (21)$$

$$R_{nl}(r) = r^{n-1}e^{-\zeta r}. \quad (22)$$

The functions $Y_{lm}(\theta, \varphi)$ are the spherical harmonic functions and ζ a parameter which describes the effective radius of the orbital. It can be calculated variationally for a specified atom and shell. These functions have the advantage that they are equivalent to hydrogenic orbitals and provide a good representation of atomic orbitals with standard ζ -values recommended by Slater [89]. They seem attractive but when it comes to large molecular systems, their integrals become computationally quite cumbersome. For this reason a more often used basis set is the Gaussian basis set, where

$$R_{nl} = r^{n-1}e^{-\zeta r^2}. \quad (23)$$

The Gaussian integrals are much faster to compute, but the disadvantage is that the Gaussian functions do not describe well even the hydrogenic radial function near $r = 0$. This can be compensated by using a larger basis set, which, in turn, can again become cumbersome.

Using the LCAO formalism, the charge density can be expanded in the individual primitive orbitals as

$$\rho(\mathbf{r}) = 2 \sum_{i\mu\nu} c_{i\mu}c_{i\nu}\phi_{\mu}(\mathbf{r})\phi_{\nu}(\mathbf{r}) = \sum_{\mu\nu} P_{\mu\nu}\phi_{\mu}(\mathbf{r})\phi_{\nu}(\mathbf{r}) \quad (24)$$

where the summations run over occupied states. We have defined the *density matrix* $P_{\mu\nu}$,

$$P_{\mu\nu} = 2 \sum_i c_{i\mu}c_{i\nu}. \quad (25)$$

In the Fourier transformation of the determinant wave function individual orbitals are transformed separately [90], and thus the momentum density of the system is simply

$$N(\mathbf{p}) = \sum_{\mu\nu} P_{\mu\nu}\chi_{\mu}(\mathbf{p})\chi_{\nu}(\mathbf{p}), \quad (26)$$

where $\chi_{\mu}(\mathbf{p})$ is the Fourier transform of the primitive orbital $\phi_{\mu}(\mathbf{r})$.

In the following, experimental and theoretical Compton profiles of He and N₂ will be presented. The wave functions were calculated using the LCAO method with the non-relativistic quantum-chemistry program DALTON [91], which provided the density matrices for each system. The program includes various Gaussian basis sets, of which the the cc-pVTZ set [92, 93] was chosen for this study. It is designed to be correlation consistent

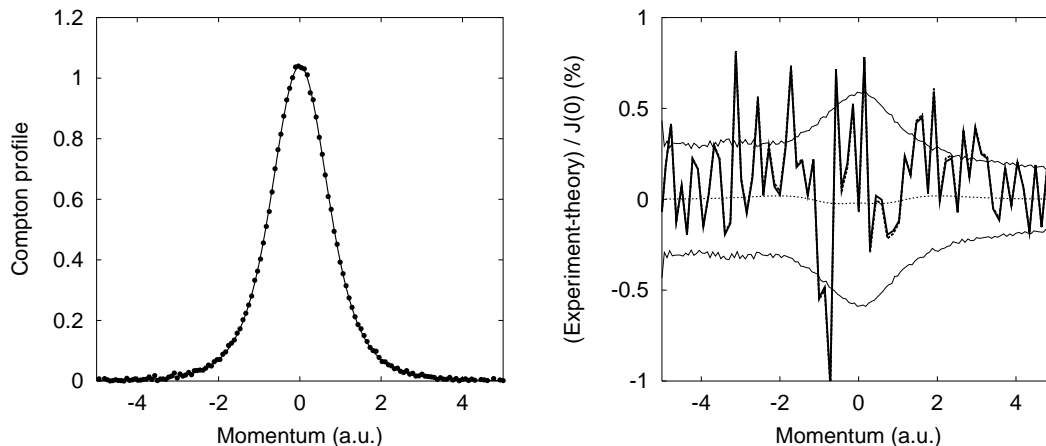


Figure 7: **Left panel:** Compton profiles of helium. Experimental data are represented by the dots, with error bars smaller than the symbol size. Two theoretical profiles are also depicted, a solid line including correlation effects and a dashed line neglecting them, but they cannot be distinguished from each others within the line thickness. **Right panel:** The difference between the experimental and theoretical Compton profiles of He. The thick solid line represents the deviation between the experimental and the theoretical cc-pVTZ Compton profiles with correlation included. The dashed line depicts similar data but without correlation correction in the theoretical profile. As in the figure in the left panel, the two lines can barely be distinguished from each other. The dotted line in the middle represents the difference between the two theoretical profiles, and the two symmetrically aligned thin solid lines represent the magnitude of the experimental errorbars.

and it is generally regarded as being capable of giving quite accurate correlation-corrected wave functions in simple systems. The momentum densities, their directional averages and finally the Compton profiles were computed from the density matrices numerically. Correlation effects were taken into account in DALTON by using the Møller-Plesset second-order perturbation theory (MP2) [94,95].

Atomic and molecular systems have been studied via Compton scattering also earlier but with much lower accuracy [81,96–100]. These studies were performed by using conventional x-ray tubes or γ -ray sources, combined with either crystal spectrometers or solid-state detectors. Most of the earlier studies that include comparisons of experimental and theoretical Compton profiles with and without correlation corrections, have obtained the theoretical profiles from different sources and the comparability of the profiles is thus questionable. In this work, the theoretical Compton profiles were calculated consistently with the same computational method using the same basis set. The correlation correction could be turned on and off easily, allowing reliable examination of the magnitude of the correlation effects in the system.

The experimental and theoretical Compton profiles of He are presented in Figure 7.

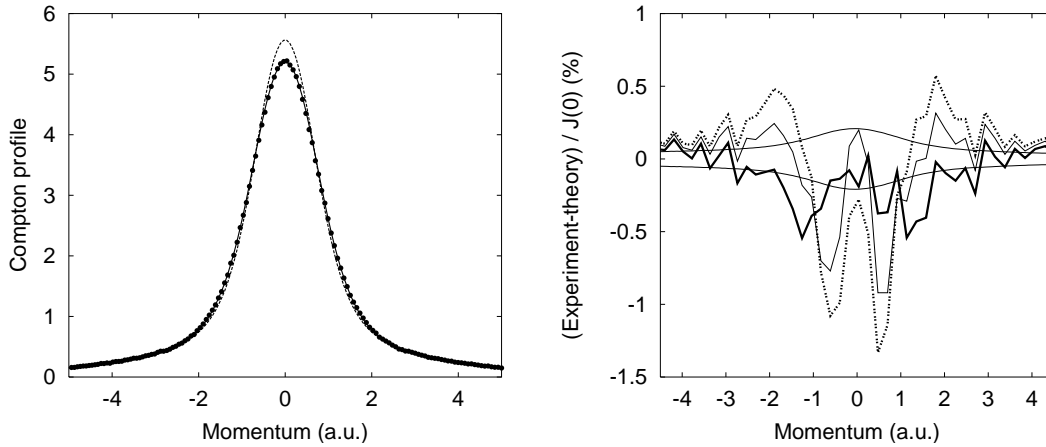


Figure 8: **Left panel:** Compton profiles of the N_2 molecule. The experimental data are presented as dots (the error bars are smaller than the symbol size) and the result of a cc-pVTZ calculation including correlation is presented as the solid line. The dashed line is the corresponding free-atom nitrogen Compton profile multiplied by a factor of two, for comparison purposes. **Right panel:** The differences between the experimental and various theoretical N_2 Compton profiles. Dashed line: cc-pVTZ without correlation; thin solid line: cc-pVTZ with correlation; thick solid line: theoretical profile by Thakkar *et al.* [101]. The two symmetrically aligned thin solid lines represent the size of the experimental errorbars.

The theoretical profiles have been convoluted with a Gaussian function with a FWHM of 0.3 a.u., representing the experimental resolution function. The agreement between experimental and theoretical Compton profiles is remarkable. From the data in the figure, it can be also concluded that correlation effects are negligible in He. It thus serves as an excellent test case for the studies of more complicated systems, since correlation effects can be ruled out as being the source of e.g. broadening of the profile.

The advantage of the Compton scattering method is that it gives quite direct information on the electron wave functions. In the **paper II** it is presented how accurate measurements of the Compton profile can be utilized to directly extract the wave function from the data, and further propose that similar studies on more complicated systems may become feasible in the future. Even if the wave function is difficult to extract directly from Compton profiles of more complicated systems, the momentum density is sensitive to wave function's phase relation on different atoms by exhibiting oscillations with frequencies which are directly connected to the bond distances. For example the hydrogen bond in ice and urea has been studied by analyzing these oscillations [24, 40].

A similar experiment to that of He was also performed on N_2 to see if correlation effects are more pronounced in this simple molecular system than they are in helium. The results of the experiment and calculations are shown in Figure 8. Again, the experimental resolution function is taken into account in the theoretical profiles. It is clearly evident

that correlation plays a more important role in N_2 than in He, and the agreement between experimental and theoretical results is enhanced when correlation is taken into account. However, even the state-of-the-art calculation by Thakkar *et al.* [101–103], explaining the system fairly well, does not give a perfect agreement with the experimental results, the experimental Compton profile being broader than the theoretical one. Multiple scattering and background radiation being ruled out in the data analysis procedure, the effect can be traced to correlation effects, which are probably not completely accounted for in the calculation.

4.2 Metals

This part of the work concentrates on metals and especially on their ground-state valence electron structure as probed by Compton scattering. One of the most important concepts in metals is the Fermi surface. It is defined as the isosurface in \mathbf{k} -space, \mathbf{k} being the wave vector of the electron and $\varepsilon(\mathbf{k})$ its energy,

$$\varepsilon(\mathbf{k}) = \varepsilon_F, \quad (27)$$

where the constant ε_F is the Fermi energy. The importance of the Fermi surface comes from the fact that all electronic transport phenomena are due to the electrons on or near the Fermi surface. For example the electric and thermal conductivities depend on the Fermi surface and on the relation $\varepsilon = \varepsilon(\mathbf{k})$.

Much of this work is devoted to the electronic structure of beryllium. It is a good candidate for electronic structure studies because of its large number of valence electrons compared to core electrons and its Fermi surface, which has a non-trivial structure but can still be calculated quite easily. It is also a very attractive target for inelastic x-ray scattering studies because of its high relative inelastic x-ray scattering cross section and low absorption. The electronic structure of Be has been studied extensively both experimentally and theoretically throughout the 20th century [13, 104–112], but the present accuracy has never before been achieved by Compton spectroscopy.

Free and non-interacting electron gas

It is not surprising that the simplest approximation for electron gas is the assumption that the electrons are non-interacting and experience only a constant potential. What really *is* surprising is that how well this approximation works in simple metals. The only really important interaction that has to be taken into account to the free electron gas theory is the Pauli exclusion principle; two electrons can not be in the same state

described by the wave vector \mathbf{k} and the spin \mathbf{s} , i.e. the electrons obey the Fermi-Dirac statistics. The probability for a state with wave vector \mathbf{k} to be occupied follows the Fermi-Dirac occupation number function, μ being the chemical potential, or the Fermi energy in the low-temperature limit,

$$n(\varepsilon) = \frac{1}{1 + e^{(\varepsilon - \mu)/kT}}, \quad (28)$$

which reduces in the low-temperature limit to a step function

$$n(\varepsilon) = \begin{cases} 1, & \varepsilon \leq \varepsilon_F \\ 0, & \varepsilon > \varepsilon_F \end{cases} \quad \text{or} \quad n(k) = \begin{cases} 1, & k \leq k_F \\ 0, & k > k_F. \end{cases} \quad (29)$$

The momentum-space form $n(k)$ is the most often used one, although it is well-defined only for homogeneous electron gas. In the metallic density region the approximation (29) is valid in solid-state systems, since the Fermi temperatures of metals are $\sim 10^4$ K; well above the melting point of most metals.

Real metals

In real metals there are two important issues that are not taken into account in the model described above, namely correlation and electron-ion interaction.

Correlation

Correlation has an effect on the momentum density of electrons that is in a way similar to the effect of finite temperature, i.e. it causes part of the momentum density to be shifted to higher momenta. However, the discontinuity apparent in the Fermi-Dirac occupation number remains, but its height is renormalized by a factor of Z_F [113, 114], as presented in Figure 9. Several different approximations have been used to calculate this effect quantitatively (i.e. to find Z_F as a function of the electron gas density) [115–120]. Some of the results for Z_F are presented in Figure 10, where the renormalization parameter is plotted as a function of $r_s = \sqrt[3]{3/4\pi\rho}$, where ρ is the electron gas density.

The extraction of Z_F from Compton scattering data has given puzzling results. One of the first results of high-resolution Compton scattering studies by Schülke *et al.* [44] was that the renormalization parameter for Li would be $Z_F \approx 0.0$ – 0.2 , by far smaller than any of the theoretical predictions depicted in Figure 10. On the other hand, a recent experiment by Suortti *et al.* suggested that $Z_F \approx 0.7$ – 0.8 for Al [32], which would be consistent with the calculations. It has been pointed out [121] that the results are largely affected by the choice of the model for $n(k)$ and not only by the values of $Z_F(r_s)$. As

a complementary study of this effect, a Compton-scattering experiment on the valence electrons of Na was carried out as described in the **paper III**. By utilizing a high pressure (up to 4.2 GPa) the free-electron gas density, and thus also r_s and the Fermi momentum, were changed directly.

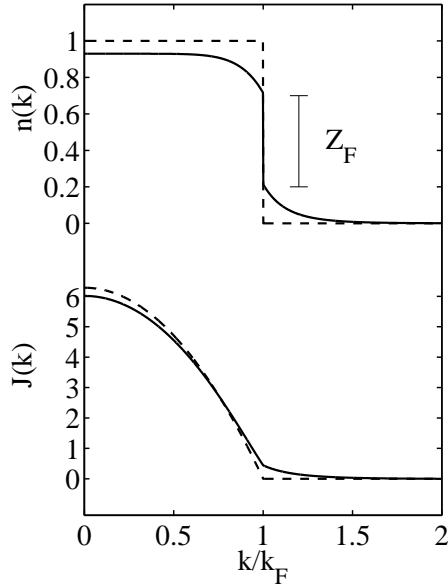


Figure 9: Example of how correlation modifies the Fermi-Dirac occupation number and the Compton profile of a free-electron gas. The utilized analytical approximation to $n(k)$ with correlation is taken from Schülke *et al.* [44], using the renormalization parameter $Z_F = 0.5$. The occupation number and the Compton profile drawn with a solid line include correlation effects, and correspondingly the curves drawn with a dashed line neglect them.

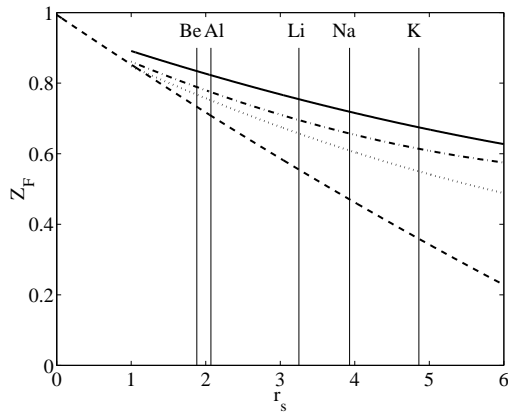


Figure 10: Renormalization parameter Z_F as a function of r_s . The dashed curve is the RPA theory [117], dotted curve by Pajanne *et al.* [117], dash-dotted curve by McDonald *et al.* [118], and the solid line by Lantto [119]. Some typical metallic densities are designated by vertical lines, ranging from $r_s = 1.88$ (Be) to $r_s = 4.86$ (K).

Because the core-electron Compton profiles are not significantly affected by the pressure, it is possible to subtract their contribution by simply observing the relative change of the total Compton profiles as a function of pressure. Thus all contamination sources, e.g. background, multiple scattering, and the asymmetry of the core-electron Compton profiles due to the failure of IA, are canceled out and purely a signal from the valence electrons remains.

The most obvious change in the Compton profiles as a function of pressure was the change of the Fermi momentum as the electron-gas density was changed. This effect is quite accurately described by the non-interacting electron-gas theory, and thus does not carry information on correlation. The magnitude of the correlation effects on the difference profiles was of the order of the statistical accuracy of the experiment [122]. Although the results are still inconclusive, the work done here is a novel experiment proving that high-pressure Compton scattering studies are possible, and the work will continue in future.

Electron-ion interaction

When the interaction between the electrons and the ions is taken into account, the momentum density gets increasingly complicated, as the periodic lattice modifies the Fermi surface. One of these effects is the formation of the so-called *high-momentum components*, which are schematically presented in the Figure 11. Their origin can be seen if the periodic lattice is written in its Fourier series representation

$$V(\mathbf{r}) = \sum_{\mathbf{G}} V_{\mathbf{G}} e^{i\mathbf{G}\cdot\mathbf{r}}, \quad (30)$$

and the corresponding wave function

$$\psi_{\mathbf{k},\nu}(\mathbf{r}) = \sum_{\mathbf{G}} a_{\nu}(\mathbf{k} + \mathbf{G}) e^{i(\mathbf{k}+\mathbf{G})\cdot\mathbf{r}}. \quad (31)$$

The electron momentum density comes out then as

$$N(\mathbf{p}) = \sum_{\mathbf{k},\nu,\mathbf{G}} |a_{\nu}(\mathbf{k} + \mathbf{G})|^2 n_{\nu}(\mathbf{k}) \delta_{\mathbf{k}+\mathbf{G},\mathbf{p}/\hbar}. \quad (32)$$

From this formulation it is evident that there are components of the momentum density centered around reciprocal lattice vectors \mathbf{G} . These are the high-momentum components, which can be described by Bragg scattering of the electron wave functions in the periodic lattice potential. The reason why they are of interest is due to the fact that they can give additional information on the lattice potential and especially on the effects of thermal disorder on the electron wave functions. Unfortunately their contribution to the Compton profiles of metals is rather small, making their direct observation quite challenging. However, even when they cannot be distinguished directly, their signal overlaps with the valence and core-electron Compton profiles, making the knowledge of the high-momentum components crucial if one wants to extract the occupation number function $n(k)$ from the Compton scattering signal of metals, as described earlier.

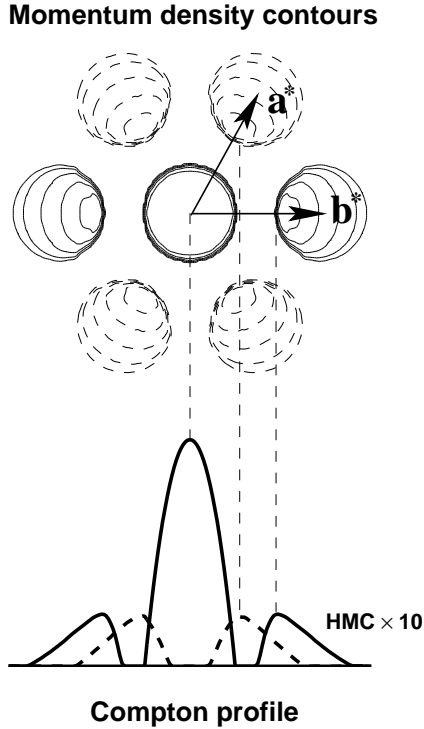


Figure 11: Outline of the formation of the high-momentum components (HMC) in a metal with a hexagonal symmetry, neglecting correlation. In the upper panel the momentum density contours centered in the middle represent the primary Fermi sphere, whereas the secondary Fermi spheres are centered around the reciprocal lattice vectors of type [100] (e.g. \mathbf{a}^* and \mathbf{b}^*). In the lower panel the corresponding Compton profile is shown. The high-momentum components are exaggerated by a factor of ten. The Compton profile peaks drawn with the dashed line are the contributions from the four high-momentum components drawn with a dashed line in the upper panel, and correspondingly the peaks drawn with a solid line are the contributions from the components drawn with a solid line in the upper panel.

In the experiment described in the **paper V** we were probably the first to be able to distinguish the high-momentum components directly in a Compton scattering experiment. Schülke *et al.* [44] reconstructed the three-dimensional momentum density of Li and were able to find signatures from the high-momentum components. Sternemann *et al.* [123] studied the temperature dependence of Li Compton profiles and found that the difference between Compton profiles in different temperatures exhibited a significant contribution from the temperature dependence of the intensity and position of the high-momentum components. A similar experiment was carried out to study the temperature dependence of the Compton profile of Be, especially paying attention in the high-momentum-component region (**paper V**).

The experimental results were compared to a simple heuristic pseudopotential calculation. It was found out that the temperature dependence of the high-momentum components was quite small in Be, in contrast to the results for Li, proving that thermal disorder does not play a significant role in the lattice potential modulation of the wave functions of Be valence electrons.

Correlation in inhomogeneous electron gas

The free-electron model assumes homogeneous electron gas, i.e. it neglects the interaction between the valence electrons and the ions. If there is no quantitative agreement on

the correlation effects in homogeneous electron gas, it is even more difficult to compute the effects of correlation on inhomogeneous electron gas. The correlation effect is usually taken into account within the local-density approximation (LDA) by the isotropic Lam-Platzman correction [124] using the occupation number function for interacting homogeneous electron gas. Being isotropic, this correction cannot take into account correlation effects that have anisotropic effects on the momentum density. In the **paper IV** differences were found between experimental and LDA based Lam-Platzman-corrected beryllium Compton profiles [58–60], which were previously regarded as highly accurate. The differences were direction-dependent and their magnitude was roughly twice the magnitude of the Lam-Platzman correction. While the factor of two in magnitude is still unexplained, similar results have been achieved computationally for Cr using an extension to an augmented-plane-wave (APW) scheme [125] and more recently using the *GW*-approximation [126]. A quantum-Monte-Carlo study of the correlation effects on Li [35] resulted in a correlation correction to the Li Compton profile that was very similar to the Lam-Platzman correction. Although the results for Li and Be are difficult to compare, it is evident that there is no agreement to the problem of how correlation effects should be incorporated into theoretical Compton profiles.

A motivation for studying the temperature dependence of the Compton profiles was a recent suggestion that the observed discrepancies between experimental and theoretical Compton profiles would not be due to correlation but due to thermal disorder, which would make the Compton profiles broader than anticipated [127]. Studies on lithium did not support this picture [123], and the experiment described in the **paper V** acted as a confirmation of that result for inhomogeneous electron gas. It was indeed found that thermal disorder does not broaden the Compton profiles of Be, and other reasons for the broadening must be sought, possibly originating from correlation.

5 Conclusions

This thesis describes highly accurate experimental Compton profiles and their comparison with corresponding theoretical profiles. A systematic series of experiments was carried out for He, N₂, Na and Be to study the effect of interactions mentioned in the previous section as a function of the complicity of the electronic system.

Attempts to push the experimental resolution to the level of 0.02 a.u. utilizing low-energy (10 keV) photons suggested that final-state effects smear out the Fermi surface signatures and thus the failure of the impulse approximation may prohibit accurate experiments with these low photon energies. The failure of the impulse approximation

concerning the core electrons was found to be simpler to account for, and the subtraction of the asymmetric core-electron Compton profiles was found to be feasible when the utilized incident photon energy was 30 keV or higher.

Comparing the experimental and computational results it can be concluded that correlation plays a significant role in solid-state systems. Especially the correlation effects in inhomogeneous electron gas lack an accurate theoretical description. Also some disagreement between theoretical and experimental Compton profiles of N₂ was found. Adding the effect of correlation to the theoretical profiles enhances the agreement, but even the present state-of-the-art theoretical calculations do not describe this system exactly.

This work proves the usefulness and sensitivity of Compton scattering experiments to research areas such as studies of correlation phenomena, electron-ion interaction and effects of bonding, or more generally, chemical environment. The experiments can be carried out with crystalline, liquid or gaseous samples without restrictions to pressure or temperature, so the method can be applied to studies of electronic systems in extreme conditions.

6 Summary of the papers

The publications in this thesis are examples of how modern synchrotron radiation sources give a possibility to enhance the accuracy of Compton scattering experiments. The main aspects are the electronic structure of atomic, molecular and metallic systems, especially studying the effects of correlation, electron-ion interaction, and Fermi surfaces of metals.

Paper I introduces studies of the failure of the impulse approximation as being a source of asymmetry in experimental core-electron Compton profiles. The observed asymmetry was found to be quite well explained by a QSCF method but some disagreement was found, suggesting that a better treatment to go beyond the impulse approximation is needed.

Paper II presents novel studies of the wave function of helium atom using the Compton scattering technique. The electronic structure of He is simple enough to enable the analysis of its $1s$ wave function directly from the measured Compton profile. Further studies for wave functions of more complicated systems are proposed.

Paper III presents studies of the occupation number density of Na under high pressure. A previously used method to compare electron momentum densities as a function of r_s was to measure Compton profiles of different metals, having different electron densities, but the comparison of the results is cumbersome. We presented a novel experiment to change r_s directly using the same sample material. The results show how the Fermi

energy changes as a function of r_s and the change is well explained by a simple RPA model.

Paper IV discusses the experimental Compton profiles of Be as a function of the incident-photon energy. Severe deviations from the impulse approximation were found with low photon energies (~ 10 keV) even for the valence-electron Compton profiles. With high photon energies, when the impulse approximation is valid for the valence electrons, deviations from the LDA-based theoretical Compton profiles were found, and the differences were attributed to arise from correlation effects in the ground state of the electron gas.

Paper V describes the temperature dependence of Be Compton profiles. The experimental results were compared to a pseudopotential model. It was found that thermal disorder has only little effect on the ground-state properties of the electron gas in beryllium, suggesting that the observed discrepancies between experimental and theoretical Compton profiles are due to other effects, possibly correlation.

References

- [1] A. H. Compton. Phys. Rev. **21**, 207 (1923).
- [2] J. W. M. DuMond. Phys. Rev. **33**, 643 (1929).
- [3] M. J. Cooper, J. A. Leake, and R. J. Weiss. Philos. Mag. **12**, 797 (1965).
- [4] K. Das Gupta. Phys. Rev. Lett. **3**, 38 (1957).
- [5] C. J. Sparks. Phys. Rev. Lett. **33**, 262 (1974).
- [6] E. D. Isaacs and P. Platzman. Physics Today **2**, 40 (1996).
- [7] N. Sakai. J. Appl. Cryst. **29**, 81 (1996).
- [8] M. J. Cooper, S. P. Collins, D. N. Timms, A. Brahmia, P. P. Kane, R. S. Holt, and D. Laundry. Nature (London) **333**, 151 (1988).
- [9] S. W. Lovesey and S. P. Collins. *X-Ray Scattering and Absorption by Magnetic Materials*. Oxford University Press, New York, (1996).
- [10] M. J. Cooper, R. S. Holt, P. Pattison, and K. R. Lea. Commun. Phys. **1**, 159 (1976).
- [11] R. S. Holt, M. J. Cooper, and K. R. Lea. J. Phys. E **11**, 68 (1978).
- [12] G. Loupiau, J. Petiau, A. Issolah, and M. Schneider. Phys. Stat. Sol. B **102**, 79 (1980).
- [13] K. Hämäläinen, S. Manninen, C.-C. Kao, W. Caliebe, J. B. Hastings, A. Bansil, S. Kaprzyk, and P. M. Platzman. Phys. Rev. B **54**, 5453 (1996).
- [14] S. Ragot, J.-M. Gillet, and P. J. Becker. Phys. Rev. B **65**, 235115 (2002).
- [15] D. L. Anastassopoulos, A. A. Vradis, and G. D. Priftis. Physica B: Cond. Matter **318**, 378 (2002).
- [16] T. Baruah, R. R. Zope, and A. Kshirsagar. Phys. Rev. B **60**, 10770 (1999).
- [17] E. P. Mazarakiotis, D. L. Anastassopoulos, A. A. Vradis, G. D. Priftis, Ch. Bellin, and G. Loupiau. Physica B: Cond. Matter **318**, 382 (2002).

-
- [18] A. Bansil, B. Barbiellini, S. Kaprzyk, and P. E. Mijnders. *J. Phys. Chem. Solids* **62**, 2191 (2001).
- [19] P. Suortti, T. Buslaps, V. Honkimäki, A. Shukla, J. Kwiatkowska, F. Maniowski, S. Kaprzyk, and A. Bansil. *J. Phys. Chem. Solids* **62**, 2223 (2001).
- [20] B. K. Sharma, B. L. Ahuja, R. Jain, A. Shukla, P. Suortti, J. A. Duffy, and M. J. Cooper. *J. Phys. Chem. Solids* **62**, 2233 (2001).
- [21] J. Laukkanen, K. Hämäläinen, S. Manninen, A. Shukla, T. Takahashi, K. Yamada, B. Barbiellini, S. Kaprzyk, and A. Bansil. *J. Phys. Chem. Solids* **62**, 2249 (2001).
- [22] I. Matsumoto, J. Kwiatkowska, F. Maniowski, M. Itou, H. Kawata, N. Shiotani, S. Kaprzyk, P.E. Mijnders, B. Barbiellini, and A. Bansil. *Phys. Rev. B* **64**, 045121 (2001).
- [23] J.-M. Gillet, P. J. Becker, and P. Cortona. *Phys. Rev. B* **63**, 235115 (2001).
- [24] A. Shukla, E. D. Isaacs, D. R. Hamann, and P. M. Platzman. *Phys. Rev. B* **64**, 052101 (2001).
- [25] Y. Sakurai, Y. Tanaka, A. T. Stewart, N. Shiotani, P. E. Mijnders, S. Kaprzyk, and A. Bansil. *Phys. Rev. B* **63**, 045120 (2001).
- [26] T. Ohata, M. Itou, I. Matsumoto, Y. Sakurai, H. Kawata, N. Shiotani, S. Kaprzyk, P. E. Mijnders, and A. Bansil. *Phys. Rev. B* **62**, 16528 (2000).
- [27] Y. Tanaka, K. J. Chen, C. Bellin, G. Loupiau, H. M. Fretwell, A. Rodrigues-Gonzalez, M. A. Alam, S. B. Dugdale, A. A. Manuel, A. Shukla, T. Buslaps, P. Suortti, and N. Shiotani. *J. Phys. Chem. Solids* **61**, 365 (2000).
- [28] A. Shukla, B. Barbiellini, A. Erb, A. Manuel, B. Revaz, T. Buslaps, V. Honkimäki, and P. Suortti. *J. Phys. Chem. Solids* **61**, 357 (2000).
- [29] S. B. Dugdale, H. M. Fretwell, K. J. Chen, Y. Tanaka, A. Shukla, T. Buslaps, Ch. Bellin, G. Loupiau, M. A. Alam, A. A. Manuel, P. Suortti, and N. Shiotani. *J. Phys. Chem. Solids* **61**, 361 (2000).
- [30] C. Fluteaux, J. M. Gillet, and P. Becker. *J. Phys. Chem. Solids* **61**, 369 (2000).
- [31] I. Matsumoto, J. Kwiatkowska, F. Maniowski, A. Bansil, S. Kaprzyk, M. Itou, H. Kawata, and N. Shiotani. *J. Phys. Chem. Solids* **61**, 375 (2000).

-
- [32] P. Suortti, T. Buslaps, V. Honkimäki, C. Metz, A. Shukla, Th. Tschentscher, J. Kwiatkowska, F. Maniawski, A. Bansil, S. Kaprzyk, A. S. Kheifets, D. R. Lun, T. Sattler, J. R. Schneider, and F. Bell. *J. Phys. Chem. Solids* **61**, 397 (2000).
- [33] E. D. Isaacs, A. Shukla, P. M. Platzman, D. R. Hamann, B. Barbiellini, and C. A. Tulk. *J. Phys. Chem. Solids* **61**, 403 (2000).
- [34] M. Marangolo, Ch. Bellin, G. Loupiau, S. Rabii, S. C. Erwin, and Th. Buslaps. *Phys. Rev. B* **60**, 17084 (1999).
- [35] C. Filippi and D. M. Ceperley. *Phys. Rev. B* **59**, 7907 (1999).
- [36] C. Metz, Th. Tschentscher, T. Sattler, K. Höppner, J. R. Schneider, K. Wittmaack, D. Frischke, and F. Bell. *Phys. Rev. B* **60**, 14049 (1999).
- [37] G. Stutz, F. Wohlert, A. Kaprolat, W. Schülke, Y. Sakurai, Y. Tanaka, M. Ito, H. Kawata, N. Shiotani, S. Kaprzyk, and A. Bansil. *Phys. Rev. B* **60**, 7099 (1999).
- [38] J.-M. Gillet, C. Fluteaux, and P. J. Becker. *Phys. Rev. B* **60**, 2345 (1999).
- [39] A. Shukla, B. Barbiellini, A. Erb, A. Manuel, T. Buslaps, V. Honkimäki, and P. Suortti. *Phys. Rev. B* **59**, 12127 (1999).
- [40] E. D. Isaacs, A. Shukla, P. M. Platzman, D. R. Hamann, B. Barbiellini, and C. A. Tulk. *Phys. Rev. Lett.* **82**, 600 (1999).
- [41] M. Marangolo, J. Moscovici, G. Loupiau, S. Rabii, S. C. Erwin, C. Hérold, J. F. Marêché, and Ph. Lagrange. *Phys. Rev. B* **58**, 7593 (1998).
- [42] B. Králik, P. Delaney, and S. G. Louie. *Phys. Rev. Lett.* **80**, 4253 (1998).
- [43] A. Bansil, S. Kaprzyk, A. Andrejczuk, L. Dobrzynski, J. Kwiatkowska, F. Maniawski, and E. Zukowski. *Phys. Rev. B* **57**, 314 (1998).
- [44] W. Schülke, G. Stutz, F. Wohlert, and A. Kaprolat. *Phys. Rev. B* **54**, 14381 (1996).
- [45] A. L. Robinson. *X-ray data booklet*, 2nd edition, chapter 2.2. Lawrence Berkeley National Laboratory, California (2001).
- [46] M. A. Kornberg, A. L. Godunov, S. Itza-Ortiz, D. L. Ederer, J. H. McGuire, and L. Young. *J. Synchrotron Rad.* **9**, 298 (2002).
- [47] W. Schülke. *J. Phys.: Condens. Matter* **13**, 7557 (2001).

-
- [48] M. J. Cooper. *Rep. Prog. Phys.* **48**, 415 (1985).
- [49] B. Williams, editor. *Compton scattering*. McGraw-Hill, London (1977).
- [50] M. J. Puska and R. M. Nieminen. *Rev. Mod. Phys.* **66**, 841 (1994).
- [51] F. Bell and J. R. Schneider. *J. Phys.: Condens. Matter* **13**, 7905 (2001).
- [52] E. Weigold. in *X-Ray and Inner-Shell Processes*, p. 81. AIP Conference Proceedings 506. Melville, New York (2000).
- [53] G. Kontrym-Sznajd, M. Samsel-Czekala, A. Pietraszko, H. Sormann, S. Manninen, S. Huotari, K. Hämäläinen, J. Laukkanen, R. N. West, and W. Schülke. *Phys. Rev. B* **66**, 155110 (2002).
- [54] W. Schülke. in *Handbook on Synchrotron Radiation*, Vol. 3, p. 565. Elsevier, Amsterdam (1991).
- [55] L. van Hove. *Phys. Rev.* **95**, 249 (1954).
- [56] P. Eisenberger and P. M. Platzman. *Phys. Rev. A* **2**, 415 (1970).
- [57] P. Holm. *Phys. Rev. A* **37**, 3706 (1988).
- [58] S. Kaprzyk and A. Bansil. *Phys. Rev. B* **42**, 7358 (1990).
- [59] A. Bansil and S. Kaprzyk. *Phys. Rev. B* **43**, 10335 (1991).
- [60] A. Bansil, S. Kaprzyk, and J. Tobała. in *Application of Multiple Scattering Theory in Materials Science*, p. 505. MRS Symposia Proceedings No. 253. Materials Research Society, Pittsburgh (2002).
- [61] F. Biggs, L. B. Mendelsohn, and J. B. Mann. Relativistic-orbital and entire-atom Compton profiles for the elements. Technical report, Sandia Laboratories, 1976.
- [62] A. Issolah, B. Levy, A. Beswick, and G. Louprias. *Phys. Rev. A* **38**, 4509 (1988).
- [63] A. Issolah, Y. Garreau, B. Lévy, and G. Louprias. *Phys. Rev. B* **44**, 11029 (1991).
- [64] P. Holm and R. Ribberfors. *Phys. Rev. A* **40**, 6251 (1989).
- [65] R. K. Pathak, A. Kshirsagar, R. Hoffmeyer, and A. J. Thakkar. *Phys. Rev. A* **48**, 2946 (1993).

- [66] A. Issolah, Y. Garreau, G. Loupiau, and B. Lévy. *Solid State Comm.* **84**, 1099 (1992).
- [67] B. J. Bloch and L. B. Mendelsohn. *Phys. Rev. A* **9**, 129 (1974).
- [68] F. Gasser and C. Tavard. *Phys. Rev. A* **27**, 117 (1983).
- [69] C. Sternemann, K. Hämäläinen, A. Kaprolat, A. Soininen, G. Döring, C.-C. Kao, S. Manninen, and W. Schülke. *Phys. Rev. B* **62**, R7687 (2000).
- [70] J. A. Soininen and Eric L. Shirley. *Phys. Rev. B* **61**, 16423 (2000).
- [71] J. A. Soininen and E. L. Shirley. *Phys. Rev. B* **64**, 165112 (2001).
- [72] J. A. Soininen, K. Hämäläinen, and S. Manninen. *Phys. Rev. B* **64**, 125116 (2001).
- [73] P. Suortti, T. Buslaps, P. Fajardo, V. Honkimäki, M. Kretschmer, U. Lienert, J. E. McCarthy, M. Renier, A. Shukla, T. Tschentscher, and T. Meinander. *J. Synchrotron Radiat.* **6**, 69 (1999).
- [74] P. Suortti, T. Buslaps, V. Honkimäki, M. Kretschmer, and M. Renier. *Z. Phys. Chem.* **215**, 1419 (2001).
- [75] G. Swislow. *spec*, a program for controlling scientific instruments. www.certif.com.
- [76] J. M. Besson, R. J. Nelmes, G. Hamel, J. S. Loveday, G. Weill, and S. Hull. *Physica B* **180/181**, 907 (1992).
- [77] M. Mezouar, T. Le Bihan, H. Libotte, Y. Le Godec, and D. Häusermann. *J. Synchrotron Radiat.* **6**, 1115 (1999).
- [78] A. Jayaraman. *Rev. Mod. Phys.* **55**, 65 (1983).
- [79] A. Jayaraman. *Sci. Am.* **250**, 54 (1984).
- [80] J. A. Xu and H. K. Mao. *Science* **290**, 783 (2000).
- [81] T. Paakkari and M. Merisalo. *Chem. Phys. Lett.* **53**, 313 (1978).
- [82] E. Erola, V. Eteläniemi, P. Suortti, P. Pattison, and W. Thomlinson. *J. Appl. Cryst.* **23**, 35 (1990).
- [83] M. Alatalo, H. Kauppinen, K. Saarinen, M. J. Puska, J. Mäkinen, P. Hautojärvi, and R. M. Nieminen. *Phys. Rev. B* **51**, 4176 (1995).

- [84] S. Huotari *et al.* To be published.
- [85] D. Pines and P. Nozières. *The Theory of Quantum Liquids*. Benjamin Press, New York, 1966.
- [86] A. G. Eguiluz and W.-D. Schöne. *Mol. Phys.* **94**, 87 (1998).
- [87] E. Steiner. *The determination and interpretation of molecular wave functions*. Cambridge University Press, Cambridge (1976).
- [88] J. A. Pople and D. L. Beveridge. *Approximate Molecular Orbital Theory*. McGraw-Hill, New York (1970).
- [89] J. C. Slater. *Phys. Rev.* **36**, 57 (1930).
- [90] J. R. Epstein. *J. Chem. Phys.* **53**, 4418 (1970).
- [91] T. Helgaker, H. J. Å. Jensen, P. Jørgensen, J. Olsen, K. Ruud, H. Ågren, A. A. Auer, K. L. Bak, V. Bakken, O. Christiansen, S. Coriani, P. Dahle, E. K. Dalskov, T. Enevoldsen, B. Fernandez, C. Hättig, K. Hald, A. Halkier, H. Heiberg, H. Hettema, D. Jonsson, S. Kirpekar, R. Kobayashi, H. Koch, K. V. Mikkelsen, P. Norman, M. J. Packer, T. B. Pedersen, T. A. Ruden, A. Sanchez, T. Saue, S. P. A. Sauer, B. Schimmelpfennig, K. O. Sylvester-Hvid, P. R. Taylor, and O. Vahtrsa. Dalton, a molecular electronic structure program, release 1.2 (2001). <http://www.kjemi.uio.no/software/dalton/>.
- [92] T. H. Dunning (Jr). *J. Chem. Phys.* **90**, 1007 (1989).
- [93] D. E. Woon and T. H. Dunning (Jr). *J. Chem. Phys.* **100**, 2975 (1994).
- [94] C. Møller and M. S. Plesset. *Phys. Rev.* **46**, 618 (1934).
- [95] J. S. Binkley and J. A. Pople. *Int. J. Quantum Chem.* **9**, 229 (1975).
- [96] P. Eisenberger. *Phys. Rev. A* **2**, 1678 (1970).
- [97] P. Eisenberger and W. A. Reed. *Phys. Rev. A* **5**, 2085 (1972).
- [98] T. Paakkari and M. Merisalo. *Chem. Phys. Lett.* **33**, 432 (1975).
- [99] S. Manninen, T. Paakkari, and M. Merisalo. *Chem. Phys. Lett.* **46**, 62 (1977).
- [100] M. Cooper and B. Williams. *Phil. Mag.* **22**, 543 (1970).

-
- [101] A. J. Thakkar and H. Tatewaki. Phys. Rev. A **42**, 1336 (1990).
- [102] A. J. Thakkar, J. W. Liu, and W. J. Stevens. Phys. Rev. A **34**, 4695 (1986).
- [103] A. J. Thakkar, J. W. Liu, and G. C. Lie. Phys. Rev. A **36**, 5111 (1987).
- [104] T. L. Loucks and P. H. Cutler. Phys. Rev. **133**, A819 (1964).
- [105] P. Rennert. Phys. Stat. Sol. (b) **105**, 567 (1981).
- [106] C. Herring and A. G. Hill. Phys. Rev. **58**, 132 (1940).
- [107] M. Y. Chou, P. K. Lam, and M. L. Cohen. Phys. Rev. B **28**, 1696 (1983).
- [108] G. E. W. Bauer and J. R. Schneider. Solid State Comm. **47**, 673 (1983).
- [109] M. Y. Chou, P. K. Lam, M. L. Cohen, G. Louprias, J. Chomilier, and J. Petiau. Phys. Rev. Lett. **49**, 1452 (1982).
- [110] N. K. Hansen, P. Pattison, and J. R. Schneider. Z. Physik B **35**, 215 (1979).
- [111] M. Itou, Y. Sakurai, T. Ohata, A. Bansil, S. Kaprzyk, Y. Tanaka, H. Kawata, and N. Shiotani. J. Phys. Chem. Sol. **59**, 99 (1998).
- [112] R. Dovesi, C. Pisani, F. Ricca, and C. Roetti. Phys. Rev. B **25**, 3731 (1982).
- [113] J. M. Luttinger. Phys. Rev. **119**, 1153 (1960).
- [114] R. D. Mattuck. *A guide to Feynman diagrams in the many-body problem*. McGraw-Hill, New York, 2nd edition (1976).
- [115] E. Daniel and S. H. Vosko. Phys. Rev. **120**, 2041 (1960).
- [116] J. Lam. Phys. Rev. B **3**, 3243 (1971).
- [117] E. Pajanne and J. Arponen. J. Phys. C: Solid State Phys. **15**, 2683 (1982).
- [118] A. H. McDonald, M. W. C. Dharma-wardana, and D. J. W. Geldart. J. Phys. F: Met. Phys. **10**, 1719 (1980).
- [119] L. J. Lantto. Phys. Rev. B **22**, 1380 (1980).
- [120] Y. Takada and H. Yasuhara. Phys. Rev. B **44**, 7879 (1991).

-
- [121] W. Schülke, C. Sternemann, A. Kaprolat, and G. Döring. *Z. Phys. Chem.* **215**, 1353 (2001).
- [122] S. Huotari, K. Hämäläinen, J. Laukkanen, A. Soininen, S. Manninen, C.-C. Kao, T. Buslaps, M. Mezouar, and H.K. Mao. *Science and Technology of High Pressure* **2**, 1017 (2000).
- [123] C. Sternemann, T. Buslaps, A. Shukla, P. Suortti, G. Döring, and W. Schülke. *Phys. Rev. B* **63**, 094301 (2001).
- [124] L. Lam and P. M. Platzman. *Phys. Rev. B* **9**, 5122 (1974).
- [125] D. A. Cardwell, M. J. Cooper, and S. Wakoh. *J. Phys.: Condens. Matter* **1**, 541 (1989).
- [126] Y. Kubo. *J. Phys. Chem. Solids* **62**, 2199 (2001).
- [127] S. B. Dugdale and T. Jarlborg. *Solid State Commun.* **105**, 283 (1998).